

Nanoscale

Accepted Manuscript



This is an *Accepted Manuscript*, which has been through the Royal Society of Chemistry peer review process and has been accepted for publication.

Accepted Manuscripts are published online shortly after acceptance, before technical editing, formatting and proof reading. Using this free service, authors can make their results available to the community, in citable form, before we publish the edited article. We will replace this *Accepted Manuscript* with the edited and formatted *Advance Article* as soon as it is available.

You can find more information about *Accepted Manuscripts* in the [Information for Authors](#).

Please note that technical editing may introduce minor changes to the text and/or graphics, which may alter content. The journal's standard [Terms & Conditions](#) and the [Ethical guidelines](#) still apply. In no event shall the Royal Society of Chemistry be held responsible for any errors or omissions in this *Accepted Manuscript* or any consequences arising from the use of any information it contains.



Electrostatic gating in carbon nanotube aptasensors

Han Yue Zheng,^{ab} Omar A. Alsager,^{ab} Bicheng Zhu,^c Jadranka Travas-Sejdic,^{bc} Justin M. Hodgkiss^{ab} and Natalie O. V. Plank^{*ab}

Received 00th January 20xx,
Accepted 00th January 20xx

DOI: 10.1039/x0xx00000x

www.rsc.org/

Synthetic DNA aptamer receptors could boost the prospects of carbon nanotube (CNT)-based electronic biosensors if signal transduction can be understood and engineered. Here, we report CNT aptasensors for potassium ions that clearly demonstrate aptamer-induced electrostatic gating of electronic conduction. The CNT network devices were fabricated on flexible substrates via a facile solution processing route and non-covalently functionalised with potassium binding aptamers. Monotonic increases in CNT conduction were observed in response to increasing potassium ion concentration, with a level of detection as low as 10 picomolar. The signal was shown to arise from a specific aptamer-target interaction that stabilises a G-quadruplex structure, bringing high negative charge density near the CNT channel. Electrostatic gating is established via the specificity and the sign of the current response, and by observing its suppression when higher ionic strength decreases the Debye length at the CNT-water interface. Sensitivity towards potassium and selectivity against other ions is demonstrated in both resistive mode and real time transistor mode measurements. The effective device architecture presented, along with the identification of clear response signatures, should inform the development of new electronic biosensors using the growing library of aptamer receptors.

Introduction

Field-effect transistors (FETs) offer an intrinsic signal amplification platform for building biosensors that produce a strong electrical response in the presence of specific analytes.^{1,2} Creating effective FET biosensors requires coupling favourable properties of active semiconducting materials and of biological recognition elements - a combination that can prove difficult to achieve.

Carbon nanotube (CNT) network films offer a highly attractive semiconducting platform for FET device applications. Their desirable properties include; reported mobilities of 2 - 5 cm²/V·s and high ON/OFF ratios of ~2000 that are maintained in FET measurements in aqueous environments,³ routes to non-destructive surface functionalization of the CNT films,⁴ and simple, reproducible fabrication procedures.⁵⁻⁸ These properties were first exploited in detecting the interaction of biotin-streptavidin on single CNT FETs,^{9,10} and through antibody coated CNT devices for protein detection.^{2,4} However, this approach was restricted to a limited range of target proteins, and device fabrication and

operation was subject to tight constraints to maintain antibody stability. For example, the antibody receptors degrade irreversibly at temperatures above 70 °C.^{11,12}

The emergence of synthetic receptors such as DNA aptamers^{13,14} has stimulated new opportunities for CNT biosensors.¹⁵⁻¹⁷ These short strands of DNA can be generated via a synthetic evolution process to bind with specificity for different types of targets, including cells,¹⁸ proteins,^{15,19-21} molecules,²²⁻²⁵ and even ions.²⁶⁻²⁸ Once the correct sequence for a given target is discovered, DNA aptamers can be synthesised and readily modified^{12,16} for integration in biosensor devices. One further property of DNA aptamers makes them ideally matched to CNT-based FET platforms; with their high negative charge density within a few nanometers of the CNT surface, tethered DNA aptamers are poised to gate conduction in p-type CNT channels when target binding alters the DNA conformation.^{15,20}

This simple proposal for signal transduction - FET gating via target induced changes in aptamer conformation - has been recently demonstrated in graphene devices,²⁹ but has been surprisingly difficult to realise in CNT network film devices for a number of reasons. Firstly, the need for bare CNT films (prior to aptamer functionalization) previously meant either burning off the surfactants used to enable the CNT deposition,³⁰ or directly growing CNTs on the device substrate,²⁰ with both approaches compromising the FET device characteristics. Secondly, the exposure of multiple types of interfaces and the difficulty in passivating them leaves the possibility of additional, often spurious, electrical signals. These include direct target adsorption to CNTs

^a School of Chemical and Physical Sciences, Victoria University of Wellington, Wellington 6021, New Zealand. E-mail: Natalie.Plank@vuw.ac.nz

^b The MacDiarmid Institute for Advanced Materials and Nanotechnology.

^c Polymer Electronics Research Centre (PERC), School of Chemical Sciences, University of Auckland, 23 Symonds Street, Auckland, New Zealand.

*Electronic Supplementary Information (ESI) available. See

DOI: 10.1039/x0xx00000x

leading to scattering effects and interactions at CNT/electrode interfaces modulating Schottky barriers.^{2,31,32} Finally, FET response measurements can be subject to hysteresis and drift effects, whereby signals may be influenced in large part by the measurement mode (e.g. *I-V* sweep versus real time current monitoring).

Here, we create a CNT aptasensor for detecting potassium ions. The sensor is designed with a number of features that allow us to cleanly probe the signal transduction mechanism without interference from the effects described above. First, the potassium aptamer was selected because potassium ions cannot participate in non-specific interactions with CNTs (e.g., hydrophobic adsorption) like organic molecules or proteins do, which also eliminates the requirement for passivation. Moreover, this DNA sequence binds ions via a tightly folded G-quadruplex structure,^{26,27} thereby ensuring that large changes in negative charge accompany target binding and can gate the conduction in the underlying CNTs, similar to the mercury sensor reported by An *et al.*²⁹ The potassium binding aptamer also enables the interaction specificity to be probed via DNA base mutations and different electrolyte mixtures. Secondly, we employ a novel surfactant-free deposition route to ensure that good quality semiconducting CNT networks are directly available for subsequent functionalization with aptamers. This low temperature fabrication route also has the advantage of delivering an aptasensor on a flexible polyimide substrate that could ultimately be printed. Third, by applying the gate field via a liquid electrolyte in a sample well that is aligned over the active FET channel – excluding the electrode interfaces – the behaviour of the CNT/solution interface occupied by aptamers can be isolated and probed as a function of electrolyte ionic strength. Finally, measurements are undertaken as both *I-V* sweeps, as well as real time current measurements as a function of potassium addition. The convergent results of both measurement modes exclude spurious effects like hysteresis and drift.

The combination of these features allows us to show that DNA aptamers can gate electrical signals in CNT FETs when binding induces changes in the negative charge density of DNA at the CNT interface. Electrical measurement of potassium ions is of biological interest due to the physiological function of potassium ions including regulation of blood pressure, controlling muscular functions and maintaining osmotic pressure or enzyme activations.^{26–28,33} The sensor platform presented here can also be readily applied to other targets by simply employing different aptamer sequences.

Experimental

Carbon nanotube field effect transistor fabrication

Carbon nanotube thin film transistors were fabricated through a surfactant free solution-processing route using polyimide (Kapton) as the flexible substrates. Initially a CNT suspension was produced in anhydrous 1,2-dichlorobenzene (DCB) (Sigma Aldrich). A sharp tweezer tip amount of 99% IsoNanotube-S CNTs bucky paper (NanoIntegris) was dispersed into 5 ml DCB solvent and sonicated for 1 hour to create a uniform suspension where there were no

obvious particles visible to the naked eye. Polyimide films (127 μm , Lohmann technologies Ltd) were cut into 1.4 cm by 1.4 cm substrates before cleaning by sonication in acetone for 3 minutes and followed by thoroughly rinsing in IPA and drying in clean N_2 . In order to functionalise the polyimide surface, a polydimethylsiloxane (PDMS) (Sylgard 184) stamping method was used to transfer a thin layer of thiolpyridine on the polyimide substrates.⁶ The thiolpyridine functionalised polyimide substrates were then submerged into the premade CNT DCB suspension for 2 hours before cleaning in ethanol for 5 minutes and drying in clean N_2 .

After submersion the entire polyimide substrates were coated with uniform CNT thin films. Areas of CNT thin films, 100 μm (width) by 300 μm (length), were left at controlled locations defined by photolithography (Karl Suss MJB3) and an O_2 plasma etch (Oxford Plasmalab 80 Plus) at 600 mTorr, 200 watts, 40 sccm O_2 flow, etch time 3 minutes. A further photolithography step was carried out to define the source and drain electrodes with of 5 nm Cr and 35 nm Au deposited (Angstrom Engineering Nexdep) directly onto the CNT thin films. After a lift-off process, the channel lengths of CNT FETs on the Kapton substrates were 40 μm and the channel widths were 100 μm . Atomic force microscopy (AFM) (Nanosurf, NaioAFM) was used to determine the morphology of the CNT films on polyimide substrates.

The electrodes were then encapsulated to avoid leakage currents and electrode damage in the aqueous sensing environment. AZ1518 photoresist (Microchemicals) was patterned before baking the CNT FETs at a 200°C on a hot plate in air. The active exposed area of CNT films is 10 μm length by 100 μm width. The flexible CNT FETs were then ready for chemical functionalization to fabricate the aptasensors.

Aptamer functionalisation

To immobilise aptamers on the surface of the CNTs, 1-pyrenebutanoic acid, succinimidyl ester (PBASE) was used as a linking unit that localises on the hydrophobic surface of the CNTs, while providing a reactive leaving group that can form an amide bond with the amine terminated aptamers. PBASE (95% purity) from Sigma Aldrich was exposed to the CNTs by submerging the entire device in a 1 mM PBASE methanol solution for 1 hour.^{4,34} The PBASE methanol solution was prepared by sonication in a water bath for 1 minute before use. After PBASE functionalization any excess PBASE was removed by rinsing three times in pure methanol before finally dipping in deionised (DI) water for 5 seconds. DI water for all measurements was obtained from an in house Sartorius filtration system and had a resistivity of 18.2 M Ω . The samples were then dried in clean N_2 .

Table 1. DNA sequences

Aptamer	Sequence
Potassium aptamer	5'-NH ₂ -TTTGGTTGGTGTGGTTGGTTT-3'
Non-specific sequence	5'-NH ₂ -TTTGGATGATGTCGTTGGTTT-3'

All aptamers were purchased from AlphaDNA. The sequences of the 21-mer potassium aptamer and the 21-mer non-specific aptamer,

where 3 points on the sequence were altered, have been previously used for other biosensor investigations^{28,35} and are listed in Table 1. The altered bases are highlighted in red and underlined. The aptamers were hydrated in DI water and stored at -4°C when not in use. For functionalisation, the aptamers were diluted to a concentration of $1\ \mu\text{M}$ in $20\ \text{mM}$ tris-HCl buffer. The $20\ \text{mM}$ tris-HCl buffer contains $0.017\ \text{M}$ Trizma hydrochloride (reagent grade, Sigma Aldrich) and $0.025\ \text{M}$ Trizma base (reagent grade, Sigma Aldrich) in $200\ \text{mL}$ volume of DI water. Aptamers were then denatured at 70°C in an oven for 5 minutes before cooling down to room temperature.^{23,24,28} The CNT FETs were then exposed to the aptamer solution overnight. After functionalization any excess aptamers were then washed off by rinsing in $20\ \text{mM}$ tris-HCl buffer three times followed by rinsing in DI water before drying in clean N_2 .

Electrical measurements

To test the devices in a liquid environment, a handmade PDMS well was placed on top of the CNT FET to avoid liquid leakage to the probe electrodes. All electrical measurements were taken with an Agilent 4156C parameter analyser connected to the sample via micromanipulators and a Rucker and Kolls probes station. Two electrolyte concentrations of tris-HCl buffer were prepared at $2\ \text{mM}$ and $20\ \text{mM}$, respectively. The pH of the buffer is set to 7.4, to avoid any pH dependency effects.²¹ For the CNT channel conductance measurements (resistive sensor) $120\ \mu\text{L}$ volume of tris-HCl buffer was initially added into PDMS well before starting the measurements. V_{ds} was then swept from $-500\ \text{mV}$ to $500\ \text{mV}$. To prepare K^+ solutions, potassium chloride powder (bioreagent, $\geq 99\%$, Sigma Aldrich) was dissolved in tris-HCl buffer and stirred until the powder is completely dissolved. Further I - V measurements are taken 10 mins after the addition of $10\ \mu\text{L}$ of K^+ solution to the PDMS well. The concentration of potassium during these two terminal CNT conductance measurements started initially at zero K^+ , after which the K^+ in the PDMS well was varied from $1\ \text{pM}$ to $1.1\ \mu\text{M}$ (total concentration, taking into account the content in the PDMS well prior to each addition).

For real time electrical detection measurements, the CNT FET was operated as a FET with an Ag/AgCl wire acting as the gate electrode. The gate voltage was set to $0\ \text{V}$, the source-drain voltage at $100\ \text{mV}$, and time step at $1\ \text{s}$ and the drain current was measured. For these real time continuous current measurements, the active area of the gate electrode (sheathed in plastic so that only the end is exposed) was completely covered in buffer at all times to prevent the issue of an altered current response coming from a change in the active area of the gate electrode. During the K^+ response measurements, $10\ \mu\text{L}$ of K^+ solution was added to the well every 10 mins. The concentration of K^+ ions in the PDMS well was increased from $100\ \text{pM}$ to $1.1\ \mu\text{M}$. During the Na^+ response measurements, $10\ \mu\text{L}$ of Na^+ solution was added to the well every 10 mins. The concentration of Na^+ in the PDMS well was increased from $1\ \text{nM}$ to $1.1\ \mu\text{M}$. A further test was undertaken in the presence of $1.1\ \mu\text{M}$ Na^+ solution whereby $10\ \mu\text{L}$ of K^+ solution was added to the well every 10 mins, resulting in the concentration of K^+ ions in PDMS well increasing from $1\ \text{nM}$ to $110\ \text{nM}$.

Results and discussion

CNT FET fabrication and characterisation

Before investigating the effect of aptamer functionalization, bare CNT FET devices were investigated in liquid electrolyte gating configuration. Uniform CNT films were successfully fabricated on flexible polyimide substrates via the CNT suspension method detailed in the experimental section, as shown in an AFM image in Fig. 1 (a). After metallization with Au over a Cr interlayer, the CNT FET electrodes were encapsulated with photoresist to avoid leakage current through the liquid buffer. The photograph image in Fig. 1 (b) shows an encapsulated device, which can be substantially bent without suffering delamination. A schematic image of CNT FET on the polyimide substrate measured in liquid as biosensor setup is shown in Fig. 1 (c). The gate electrode Ag/AgCl is inserted in liquid as the gate electrode. One of the advantages of applying a liquid gate rather than a more traditional back-gate through a dielectric is the higher field dependence resulting from the high capacitance of the solution electrical double layer (EDL).^{36,37}

The electrical properties of four CNT FET devices on a single polyimide substrate in a liquid PBS buffer are shown in ESI Fig. S1. All four CNT FET devices behave similarly and show p-type semiconductor properties with V_{th} varying between $0.4 - 0.47\ \text{V}$. The on/off current ratios are $\sim 5 \times 10^3$ and the hole mobilities are $\sim 4\ \text{cm}^2/\text{V}\cdot\text{s}$. One of the problems with CNTs in device applications can be the tube to tube variation in electronic response.³⁸ However, by using network films from high quality initial CNTs, the average properties of the film are consistent across the device substrate.

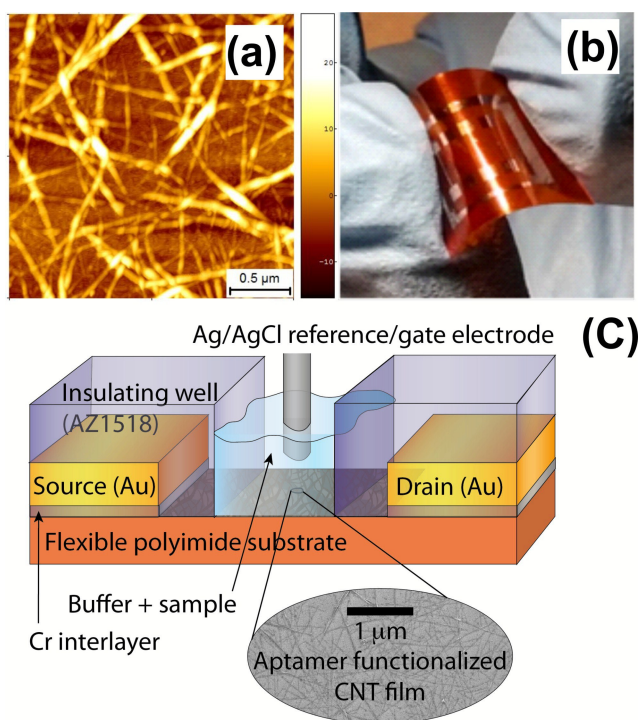


Fig. 1. A flexible CNT FET sensor platform: (a) An AFM image of the CNT film on a polyimide substrate. (b) Bendable CNT FET fabricated on a polyimide substrate, where the electrodes are encapsulated

with photoresist. (c) Schematic of the biosensor setup based on flexible CNT FET measured using liquid gating.

Carbon nanotube potassium aptasensors

In order to immobilise aptamers tethered on CNT surfaces without compromising the electronic properties of the CNTs, PBASE is used as a linking unit. As described in the experimental section, the CNT FETs are firstly submerged in methanol solution of PBASE, resulting in PBASE molecules stacking on CNT surface via non-covalent hydrophobic and π - π interactions between the carbon rings of the CNTs and the pyrene on PBASE as shown schematically in Fig. 2 (a).⁴ The advantage of this method compared to covalent functionalisation is that the carbon atoms in the CNTs retain their sp^2 hybridisation and the excellent electrical properties of the devices are maintained. The PBASE functionalised CNT FETs are then exposed to aptamer solution overnight. The amine groups ($-NH_2$) on the 5' end of aptamers are then linked onto the N-hydroxysuccinimide groups on PBASE via nucleophilic substitution,⁴ as depicted in the schematic in Fig. 2 (b). The aptamers are negatively charged due to the phosphate groups (PO_4^-) of the DNA backbone.³⁹ The tethering of the aptamers to the CNT films via the PBASE functionalisation brings these negative charges close to the CNT surfaces, causing an alteration to the electrical double layer of the device.^{15,19,20} Without amine termination, aptamers cannot covalently tether to the PBASE linkers, and instead they can non-specifically adsorb to CNT surfaces via π -stacking interactions.^{25,40} Complete coverage via tethering may limit the likelihood that tethered aptamers can additionally undergo a non-specific stacking interaction. Moreover, non-specifically adsorbed aptamers do not appear to respond to potassium ions, as we show for control devices fabricated with unsuccessful coupling (see ESI. Fig. S4).

Recognition of K^+ ions is known to induce the potassium aptamer to adopt a compact G-quadruplex structure^{26,27} as illustrated in Fig. 2 (c). The free aptamer may extend up to 8.7 nm from the CNT surface, whereas the G-quadruplex structure is folded within approximately 1.5 nm of the surface.^{28,41} This conformational change significantly increases the charge density (from the negatively charged DNA) close to the CNT surface – within the EDL region.^{15,19,20} The redistribution of charges within the EDL changes the electric field experienced by the conductive CNT channel, effectively providing an additional gating mechanism. Specifically, a higher negative charge density near the surface of a p-type device will stabilise a higher concentration of positive charges (holes) in the active channel³², thereby causing the current to increase. It is this effect that is expected to result in output current variations upon specific recognition of K^+ .

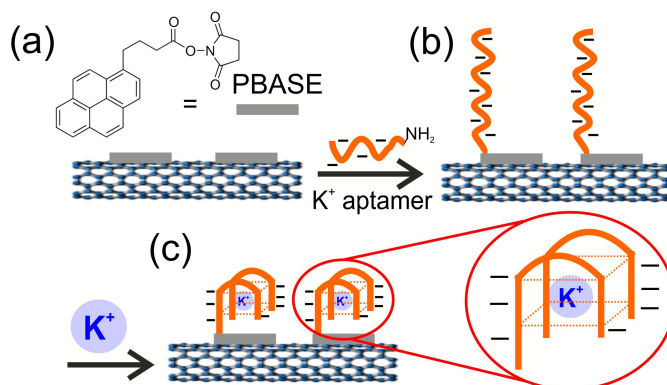


Fig. 2. The potassium aptamer functionalization process and G-quadruplex conformation after the recognition with K^+ ions: (a) PBASE stacking on CNT via PBASE, depicted in an extended conformation. (b) Potassium aptamer tethered on CNT via PBASE, depicted in an extended conformation. (c) G-quadruplex conformation^{26,27} after the recognition of K^+ ions.

Before the utilization of CNT FET aptasensors for K^+ detection, the transfer characteristics of a pristine CNT FET is compared with the aptamer functionalised CNT FET as shown in Fig. 3. A positive shift in the threshold voltage and an increase in current are observed after aptamer immobilization on the CNTs. The negatively charged aptamers induce additional positive charges in the CNTs, shifting the threshold voltage due to a surface interaction that can be considered equivalent to p-doping the FET.^{15,32} An increase in current is also observed here which may be due to the aptamer coating altering the CNT-CNT junctions in the device. This provides evidence that the aptamers are successfully tethered on the CNTs as depicted in Fig. 2 (b). Both measurements shown in Fig. 3. were carried out at the same voltage range and sweep rate. The larger hysteresis gap observed in the aptamer functionalised CNT FET could be due to increased charge screening affecting the gating properties of the EDL post aptamer immobilization. The occurrence of hysteresis in CNT FET devices is common and is part of the motivation for carrying out sensing measurements in two different operation modes.

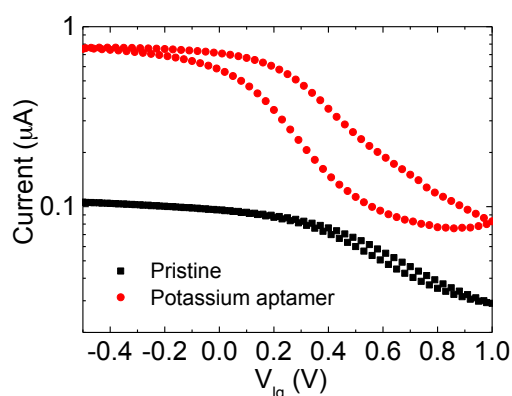


Fig. 3. Transfer characteristics of a pristine CNT FET and CNT FET being functionalised by potassium aptamers: $V_{ds} = 100$ mV, electrolyte gated in 2 mM tris-HCl.

The CNT aptasensor devices can be operated in two different operation modes. First, in the two terminal resistive measurement mode, a voltage is swept between the source and drain electrodes

and the subsequent resistance changes due to the presence of the analyte is calculated from each individual I - V curve. Secondly, signals can be measured in real time where the device is run as a FET at constant gate and source-drain potentials and the transfer current is continuously monitored during the addition of analytes.

Resistive aptasensors and the influence of Debye length. Resistive aptasensors are a clean way to explore the sensing mechanism and to probe the influence of the Debye length. In order for aptamer conformational changes to influence the electric field at the CNT channel, the aptamer charge redistribution must occur within the Debye length of the electrolyte. The Debye length (λ) is proportional to the reciprocal square root of the ionic strength I of the liquid by $\lambda \sim 0.32/\sqrt{I}$.^{19,42} Thus, according to the proposed model, the K^+ binding signal is expected to be suppressed for higher ionic strength solutions, if the Debye length becomes as short as the length scale of the aptamer conformational change. Based on the approximate dimensions of both forms of the potassium aptamer, we tested the response in two different buffer concentrations. In the more dilute 2 mM electrolyte buffer, the ionic strength is 1 mM and the Debye length is 10 nm, thus the effect of conformational changes of the potassium aptamer should be strongly felt at the CNT interface. On the other hand, the Debye length is only 2.4 nm for the 20 mM electrolyte buffer (17 mM ionic strength), which suggests that the effect of the potassium aptamer conformation is likely to be screened by the surrounding interfacial electrolyte, and therefore will induce weaker gating of the FET response.^{19,42} We note that these electrolyte concentrations are both within the range where the aptamer is known to bind analytes.³³ While K^+ binding constants are expected to be somewhat dependent on ionic strength, if anything, binding will be stronger within a higher ionic strength buffer due to better stabilization of the high charge density in the G-quadruplex structure.

In order to probe the effect of the electrolyte ionic strength, the resistive electrical response of the devices to varying K^+ concentrations (from picomolar to micromolar concentrations) are measured in 2 mM tris-HCl buffer (Fig. 4 (a)) and 20 mM tris-HCl (Fig. 4 (b)), respectively. We note that the added K^+ salt makes a negligible contribution to the ionic strength. In both buffer solutions the current increases (resistance decreases) with increased concentration of K^+ ions, consistent with K^+ addition ultimately causing an increase of negative charge density near the p-type CNTs. Both sets of measurements show no response to buffer where no K^+ is contained (the control test). The dependency of the I - V response to the K^+ concentration is observed to be much stronger in the presence of 2 mM tris-HCl compared to 20 mM tris-HCl.

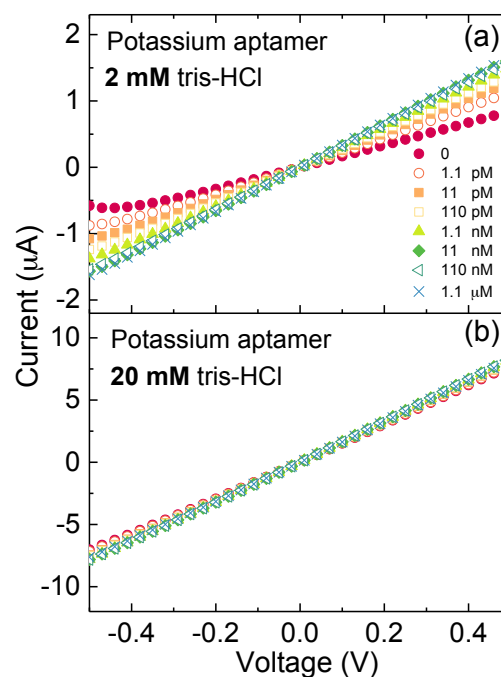


Fig. 4. Response to various concentrations of K^+ ions from potassium aptamer functionalised CNT FETs measured in (a) 2 mM tris-HCl and (b) 20 mM tris-HCl respectively. The K^+ concentrations noted in the legend apply to parts (a) and (b).

In order to compare the sensitivity of the measurement in 2 mM tris-HCl to 20 mM tris-HCl, the change in resistance, $\Delta R/R_0$, is plotted in Fig. 5. $\Delta R/R_0$ is calculated from the I - V curves in the linear range (-100 mV to +100 mV), where R_0 is resistance before exposure to K^+ ions ($[K^+] = 0$). ΔR is absolute resistance calculated by $\Delta R = R_0 - R$ where R is resistance at its corresponding K^+ concentration.²² In both buffer concentrations, the devices respond to increasing K^+ concentration between 1 pM and 11 nM before saturation is observed. However, the sensor operating in 2 mM tris-HCl shows a 7-fold stronger signal compared to the sensor operating in 20 mM tris-HCl.

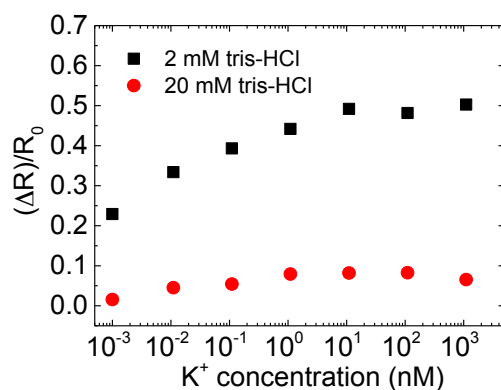


Fig. 5. The normalised resistance response ($\Delta R/R_0$) to K^+ concentration from potassium aptamer functionalised CNT FETs in 2 mM and 20 mM tris-HCl buffer solutions.

As a control we have tested the specificity of the signals by measuring the K^+ response of pristine CNT FETs (no aptamers) and CNT FET functionalised with a non-specific sequence aptamer in 2 mM tris-HCl buffer (see ESI. Fig. S2). The non-specific aptamer, whose sequence is given in Table 1, cannot easily adopt a G-quadruplex conformation to complex K^+ .^{28,35} The $\Delta R/R_0$ responses for both of these control devices alongside the working sensor is shown in Fig. 6. In contrast to the monotonically increasing current as a function of K^+ addition for the device functionalised with the correct aptamer sequence, both control devices exhibit an essentially flat response over this concentration range 1 pM–1.1 μ M. The device functionalised with the non-specific sequence does exhibit a constant offset signal for all concentrations of K^+ , with a similar magnitude to the smallest signal for the correct aptamer sequence. This offset signal indicates an additional non-specific interaction between K^+ and the negatively charged sequences. However, the concentration dependent response that is only seen with the correct aptamer sequence shows that the electronic signals in Fig. 4 (a) and Fig. 5 arise from a specific aptamer/ K^+ interaction at the CNT surface. Unlike for CNT FETs used to detect thrombin,^{15,20} IgE proteins^{19,21}, adenosine triphosphate molecules,²² or estrogen molecules²⁵ where CNT passivation is always necessary to avoid non-specific sensing via absorption onto the CNT surfaces, the K^+ aptamer CNT FETs do achieve selective detection without passivation.

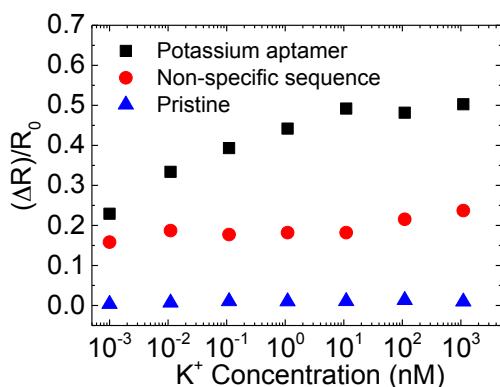


Fig. 6. The dependence of resistance on K^+ concentrations is compared between pristine CNT FET devices (triangle) and those functionalised with the potassium aptamer (squares) and the non-specific aptamer (circles).

The observation of increased current upon K^+ addition, and the suppression of K^+ binding signal in a higher ionic strength buffer strongly supports the proposed sensing mechanism: binding induces redistribution of negative charges within a few nanometres of the CNT surface, which is equivalent to p-doping, provided that this charge redistribution occurs within the Debye length of the

electrolyte. Moreover, the saturation behaviour of the two K^+ dependence curves (Fig. 6) confirms that the intrinsic aptamer- K^+ association is not substantially effected by the electrolyte ionic strength, rather, the signal transduction is altered.

Real time response. Along with the previously published work on potassium aptasensors,^{27,28,35,41,43–50} the preceding discussion of our CNT resistive sensor was not in the real time sensing mode. However, real time operation of CNT FET aptasensors can allow for the monitoring of the FET current output to show continuous changes in analyte concentration at the sensor surface, as well as confirming that the resistive response did not contain artefacts of hysteresis from sequential scans. We have successfully operated our potassium aptasensors in the real time mode to monitor dynamic changes in K^+ concentrations. The CNT FET is operated by applying a fixed source-drain voltage $V_{ds} = 100$ mV and fixed gate voltage $V_{lg} = 0$ while recording the transfer current response in real time (setup shown schematically in Fig. 1 (c)). The current response over time is compared for the potassium aptamer functionalised CNT FET (squares), the non-specific aptamer CNT FET (circles), and the pristine CNT FET (triangles) respectively, Fig. 7 (a). The measurements start with only buffer in the PDMS well. Once the current has stabilised the sensors are exposed to K^+ ions by adding 10 μ L aliquots of K^+ stock solutions into the well to produce concentrations from 100 pM (1), 1.1 nM (2), 11 nM (3), 110 nM (4) and 1.1 μ M (5). Arrows in Fig. 7 (a) indicate the points where K^+ analyte solution prepared in 2 mM tris-HCl buffer is added into the testing well. The real time measurements from the potassium aptamer functionalised flexible CNT FET show an obvious response to K^+ . The current immediately responds to the addition of K^+ at 100 pM (1), with the current continuing to increase in the presence of 1.1 nM (2), 11 nM (3), 110 nM (4) and 1.1 μ M (5) concentration of K^+ solution. In contrast to the discrete stepwise current increases observed for the device functionalised with the potassium aptamer, the control devices show a much weaker response over time. The two control devices show a slightly increasing current drift, which may be associated with the hysteresis observed in Fig. 3, and small current fluctuations (in either direction) that are presumably related to the physical disturbance at the moment of potassium addition.

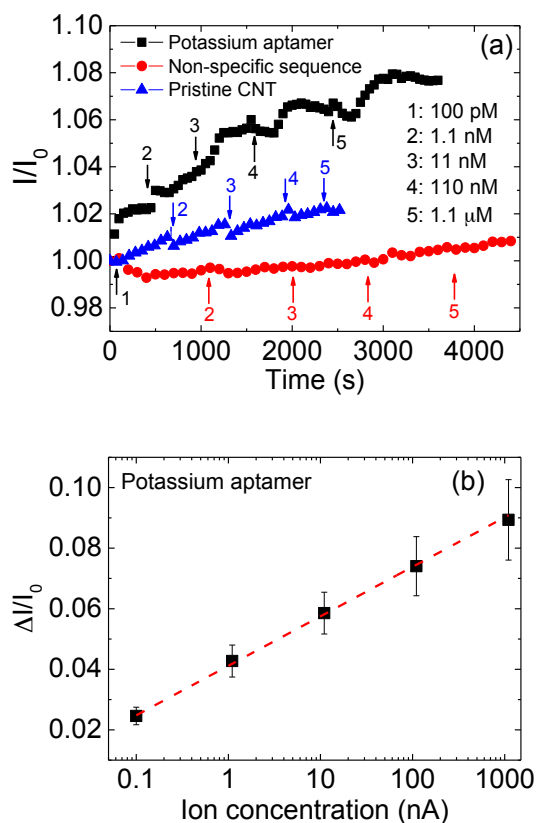


Fig. 7. (a) The real time K^+ response measured in 2 mM tris-HCl buffer from pristine CNT FET devices (triangles) and CNT FETs functionalised with either the potassium aptamer (squares), or the non-specific aptamer (circles). $V_{ds} = 100$ mV, $V_{lg} = 0$, $t = 1$ s for all devices. (b) The dependence of K^+ concentration on the current response ΔI based on real time measurement from the potassium aptamer functionalised CNT FET. Error bars are from triplicate measurements shown in the supporting information.

To quantify the current response from the real time sensor measurements, Fig. 7 (b) shows a plot of ΔI vs K^+ concentration from triplicate measurements. The current response shows a linear dependence on the logarithm of the K^+ concentration between 100 pM to 1.1 μ M, with sensitivity of 1.7% per decade. The real time CNT FET results follow the same trend as the resistive sensor described above. As both modes of sensing use devices fabricated using identical functionalization procedures, we conclude that both sensing modes are underpinned by the same electrostatic gating mechanism coupled to aptamer conformation. The experimental detectable concentration of K^+ that is achieved is 10 pM and the sensor saturated at 10 nM (linear relationship over the logarithmic concentration range between 1 pM to 10 nM) for the resistive sensor and 100 pM (linear relationship over the logarithmic concentration range between 100 pM to 1.1 μ M) for the real time sensor mode.

We also tested non-specific binding of potassium aptamer functionalised CNT FETs to Na^+ , as well as the K^+ response in the presence of 1.1 μ M Na^+ salt. Previous studies using the K^+ aptamer in different sensor formats have established its strong selectivity towards K^+ .²⁸ To confirm this selectivity in real time measurements, Na^+ solutions are firstly added into PDMS well at a varying concentration from 1 nM to 1.1 μ M and K^+ ions are then added at a varying concentration of 1 nM to 110 nM in the presence of 1.1 μ M concentration of Na^+ salt. ΔI as a function of Na^+ ion concentration (triangles) is compared with ΔI as a function of K^+ ion concentration in the presence of 1.1 μ M (circles) and the absence of Na^+ (squares) as shown in Fig. 8. The potassium aptamer functionalised CNT FETs shows a weak response to Na^+ ions. At 1 nM concentration of Na^+ ions, there is almost no response. On the other hand, 1 nM concentration of K^+ ions produces a current change of $\Delta I = 12.6$ nA when the buffer solution does not contain Na^+ , and $\Delta I = 7.3$ nA in the presence of a background 1.1 μ M Na^+ ion concentration in the buffer. At 110 nM concentration of K^+ ions, aptamer- K^+ recognition event results in a current response of 20.9 nA when no Na^+ salt is contained in the stock solution, compared to 17 nA in presence of 1.1 μ M Na^+ . We therefore conclude that K^+ recognition is not unduly influenced by Na^+ ions.

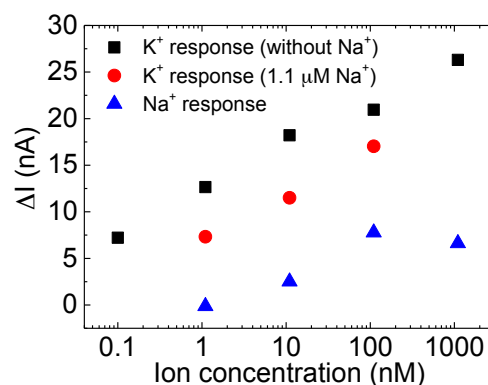


Fig. 8. The dependence of K^+ concentration on the current response ΔI based on real time measurement from the potassium aptamer functionalised CNT FETs: response to K^+ ions (absence of Na^+), K^+ ions (in the presence of 1.1 μ M Na^+ salt) and Na^+ ions.

As noted above, one advantage of our fabrication route is its compatibility with flexible substrates such as the polyimide substrates used here. We found that our sensor devices retain the electrical conduction after a bending cycle (see ESI. Fig. S5).

Aptasensors are also potentially re-useable, for example by adding a high salt concentration^{15,51,52} or rinsing in copious amounts of DI water^{53,54}. Using the more gentle latter approach, we found that the sensors lost most of their responsivity after rinsing the used devices in DI water (see ESI. Fig. S6).

Discussion

The electrostatic gating mechanism for interpreting biosensing signal response based on functionalised CNT transistor devices has

been discussed by Heller *et al.*³² Heller also summarised another three common mechanisms of biosensing by absorption of proteins on a single CNT FET model: Schottky barrier alteration, changes to the capacitance of the liquid due to the analytes affecting the ionic strength of the media, and the charge scattering effect.³² However, none of these other three mechanisms can explain the increased current response in our aptasensors. None of these effects require participation of the aptamer, and they can be ruled out by observing the baseline response to K^+ over the same concentration range for pristine CNT devices lacking the aptamer or with the non-specific aptamer in Fig. 6, along with the weak response to Na^+ (Fig. 8). The sensing response is shown to be specific to the aptamer-target interaction. Additionally, none of these other non-specific effects are to be expected in this system. In our devices, the electrodes are completely encapsulated by photoresist, therefore the Schottky barrier heights of the contacts cannot be easily influenced by the analytes. Secondly, the capacitance of the liquid cannot be substantially affected by low K^+ concentrations ($< 1.1 \mu M$) when the ionic strength of the electrolyte is several orders of magnitude higher. Only at very high concentration K^+ ($> 100 \mu M$) do we start observing a decreased current, including for pristine CNTs without aptamers, due to the added K^+ salt increasing the ionic strength and capacitance of the liquid.^{20,32,55} Finally, for small molecule detection at low concentration, the scattering effect is also suppressed. When CNT FETs are used to detect large proteins such as thrombin^{15,20} and IgE^{19,21} or high concentration of analytes,^{20,32} a reduced current (increased resistance) can be caused by scattering of the charges on the CNT sidewalls. The proteins, or molecules, physically hinder the hole transportation along the CNT by acting as charge scattering sites and increase the resistance. However, there is no evidence the analyte *increasing* the resistance in our devices, rather potassium ions *decrease* the measured resistance. The conformational coupled electrostatic gating effect is the most likely signal transduction mechanism for our aptasensors, explaining the increased current due to the redistribution of the negative charges from the G-quadruplex structure of aptamers.

The importance of Debye length for these devices to operate as successful sensors is therefore critical, as all conformational changes must take place within the EDL in order for a signal to be transduced. Previous work by Stern *et al.* in the biotin/streptavidin system showed that the real time current signal from nanowire FETs was suppressed in high concentrations of PBS buffer, highlighting the importance of ionic strength for ensuring that binding interactions are felt in the conductive channel.⁴² Our small ion detection system is equally as susceptible to the correct ionic strength, since the aptamer conformational changes that produce the signal occur within a few nanometers of the surface.

Other real time CNT FET aptasensors have been used to detect the large protein IgE, which produced ΔI values of less than 2 nA with 250 pM analyte.⁵⁶ In spite of our small target whose only mechanism for transducing signals is by the conformational gating effect, our aptasensor shows higher sensitivity and a lower detection limit than the protein system. To date, only one other study has used real time detection for a small molecule target. Lee *et al.* achieved a detection limit of 10 fM for the small molecule bisphenol A (BPA) using CNT FET aptasensors.⁵⁷ However, the lower detection limit and higher signal amplitudes in that case were achieved from a multistep labelling protocol where target molecules (BPA) were pre-labelled by secondary aptamers with a biotin-modified terminus.⁵⁷ The present work is the first example of label-free real time small molecule ($/ion$) detection using CNT FET aptamer biosensors.

We can compare our K^+ detection results to other types of K^+ aptasensors, as shown in Table 2. Our resistive mode CNT aptasensors show a clear electrical response to the presence of 10 pM K^+ in 2 mM tris-HCl buffer. This level of detection is lower than most of the previously published K^+ detection based on potassium aptamers using electrical voltammetry,^{27,47,49} impedance spectroscopy,^{27,28,41} fluorescence,^{43–46} and colorimetric analysis.⁴⁸ In both detection modes, our sensor responds pM detection limit is substantially lower than the dissociation constant of the aptamer itself ($K_d = 238 \text{ nM}^{28}$). It is surprising that in both resistive and real

Table 2. Comparison of K^+ detection in various aptasensor formats

Platform	Measurements	LOD (M)	Dynamic range (M)	Real time	Year & ref
Au electrode	Voltammetry/ EIS	1×10^{-4}	1×10^{-4} to 1×10^{-3}	no	2006 ²⁷
OliGreen dye labelled	Fluorescence	7.5×10^{-8}	1×10^{-7} to 1×10^{-6}	no	2008 ⁴³
Pyrene labelled	Fluorescence	5×10^{-4}	6.3×10^{-4} to 1×10^{-3}	no	2010 ⁴⁴
Zinc phthalocyanine	Fluorescence	8×10^{-7}	8×10^{-7} to 1×10^{-5}	no	2010 ⁴⁵
fluorescein amidite labelled	Fluorescence	4.5×10^{-9}	4×10^{-8} to 1×10^{-6}	no	2012 ⁴⁶
Fluorophore and quencher labelled	Photoluminescence	1.5×10^{-9}	5×10^{-9} to 3×10^{-8}	no	2012 ³⁵
Au electrode	Voltammetry	1×10^{-10}	1×10^{-10} to 5×10^{-8}	no	2013 ⁴⁷
Au electrode	EIS	1×10^{-10}	1×10^{-10} to 1×10^{-3}	no	2013 ⁴¹
Au nanoparticles	Colorimetric	5×10^{-9}	5×10^{-9} to 1×10^{-6}	no	2013 ⁴⁸
Au electrode	Voltammetry	1×10^{-10}	1×10^{-10} to 1×10^{-7}	no	2014 ⁴⁹
Nanochannel	Time-course of current	5×10^{-6}	5×10^{-6} to 1×10^{-3}	no	2014 ⁵⁰
Nanoporous conducting polymer electrode	EIS	1.5×10^{-14}	2×10^{-14} to 1×10^{-3}	no	2015 ²⁸
Carbon nanotubes	Chemiresistor current	1×10^{-11}	1×10^{-12} to 1×10^{-8}	no	This work
Carbon nanotubes	Transistor current	1×10^{-10}	1×10^{-10} to 1.1×10^{-6}	yes	This work

time modes, the sensor produces a strong response in the picomolar range, where one would expect a very low fraction of bound aptamers. This observation suggests strong signal enhancement, and may also indicate that either the K_D or the local ion concentration is substantially different at the solution interface than in the bulk.

Only recently has a K^+ detection limit lower than our value of 10 pM been reported for potassium aptamer based sensors. Zhu *et al.*²⁸ achieved a 20-fM detection limit using the same aptamer sequence coupled to a nanoporous conducting polymer electrode, with the signal detected via electrochemical impedance spectroscopy (EIS). The electrochemical approach was previously also found to deliver exceptionally low (femtomolar) detection limits in aptasensors for 17 β -estradiol and adenosine, which is orders of magnitude lower than other sensors using the same aptamer sequences, and also orders of magnitude lower than the K_D .²⁸ The higher detection limit of our FET-based sensor compared with the electrochemical impedance sensor using the same potassium aptamer suggests the electric field associated with aptamer conformational changes is more strongly felt by solution redox probes approaching the interface than by charge carriers in the CNT channel. Although a low detection limit is realised with the EIS sensor (10^{-14} M),²⁸ real time detection was not obtained. Compared to previously known K^+ aptasensors in Table 2, our method based on CNT FETs have exhibited advantages. K^+ quantitation is achieved with low detection limits for both resistive and real time mode sensors. Since the real time mode produces an immediate signal, aptasensors fabricated on CNT FETs may be useful for clinical diagnosis or monitoring applications. While the detection limit is substantially lower than required for K^+ quantitation in human blood (present in 3.5 – 5.5 mM concentrations²⁸), when applying this sensor platform to this and other targets is still desirable have excess detection ability so that samples may be diluted into well-defined buffers.

Conclusions

Aptamer functionalised CNT FETs were investigated as sensors for K^+ detection. The CNT network devices were fabricated via a facile, surfactant-free procedure compatible with low-cost flexible substrates. Two sensing modes were investigated using these devices: resistive sensors and FET mode for real time current output. The measurement modes resulted in detection limits of 10 pM and 100 pM, respectively. In both cases, K^+ recognition produced an increase in current. This signal could be conclusively attributed to the specific aptamer-target interaction on the CNT surfaces; comparable signals were not observed in controls including exposure to Na^+ ions, or exposure of K^+ to unfunctionalised CNT devices and devices functionalised with non-specific aptamer sequences for K^+ detection. Moreover, the response to K^+ is maintained in a background of Na^+ ions. The current response of the CNT FET aptasensor is shown to arise from an electrostatic gating effect whereby the conformational change of negatively charged aptamers within a few nanometers of the CNT surface is

equivalent to p-doping. This signal transduction mechanism requires that conformational changes occur within the Debye length. Accordingly, we show that the signal is suppressed by 7-fold when the Debye length is decreased via increasing the ionic strength of the buffer by 10-fold. To the best of our knowledge, this is the first realization of real time electronic detection of low K^+ concentrations, and the first label-free real time FET based aptasensor. The effective device architecture presented, along with the identification of clear response signatures, should inform the development of new electronic biosensors using the growing library of aptamer receptors.

Acknowledgements

HZ thanks the Victoria University of Wellington and the Chinese Government joint Scholarship. NP thanks the Foundation for Research Science and Technology project number VICX0911 and the Marsden fund, project number E1728. OA acknowledges a fellowship from King Abdulaziz City for Science and Technology. JTS and BZ thank the Ministry of Business, Innovation and Employment for the financial support (UOAX1201).

References

- 1 J. Kong, N. R. Franklin, C. Zhou, M. G. Chapline, S. Peng, K. Cho, and H. Dai, *Science* **287**, 622 (2000).
- 2 R. J. Chen, H. Cheul Choi, S. Bangsaruntip, E. Yenilmez, X. Tang, Q. Wang, Y.-L. Chang, and H. Dai, *J. Am. Chem. Soc.* **126**, 1563 (2004).
- 3 D. Fu, H. Okimoto, C.W. Lee, T. Takenobu, Y. Iwasa, H. Kataura, and L.-J. Li, *Adv. Mater.* **22**, 4867 (2010).
- 4 R. J. Chen, Y. Zhang, D. Wang, and H. Dai, *J. Am. Chem. Soc.* **123**, 3838 (2001).
- 5 E. S. Snow, J. P. Novak, P. M. Campbell, and D. Park, *Appl. Phys. Lett.* **82**, 2145 (2003).
- 6 N. O. V. Plank, M. Ishida, and R. Cheung, *J. Vac. Sci. Technol. B Microelectron. Nanom. Struct.* **23**, 3178 (2005).
- 7 N. Rouhi, D. Jain, K. Zand, and P.J. Burke, *Adv. Mater.* **23**, 94 (2011).
- 8 N. Rouhi, D. Jain, and P.J. Burke, *ACS Nano* **5**, 8471 (2011).
- 9 M. Shim, N.W. Shi Kam, R. J. Chen, Y. Li, and H. Dai, *Nano Lett.* **2**, 285 (2002).
- 10 A. Star, J. P. Gabriel, K. Bradley, and G. Gruner, *Nano Lett.* **3**, 459 (2003).
- 11 C.-C. Chen, Y.-Y. Tu, and H.-M. Chang, *J. Food Sci.* **65**, 188 (2000).
- 12 S. D. Jayasena, *Clin. Chem.* **45**, 1628 (1999).
- 13 C. Tuerk and L. Gold, *Science* **249**, 505 (1990).
- 14 A. D. Ellington and J. W. Szostak, *Nature* **346**, 818 (1990).
- 15 H.-M. So, K. Won, Y. H. Kim, B.-K. Kim, B. H. Ryu, P. S. Na, H. Kim, and J.-O. Lee, *J. Am. Chem. Soc.* **127**, 11906 (2005).
- 16 J.-O. Lee, H.-M. So, E.-K. Jeon, H. Chang, K. Won, and Y. H. Kim, *Anal. Bioanal. Chem.* **390**, 1023 (2008).
- 17 N. Yang, X. Chen, T. Ren, P. Zhang, and D. Yang, *Sensors Actuators*

- B Chem. **207**, 690 (2015).
- ¹⁸ J. K. Herr, J. E. Smith, C. D. Medley, D. Shangguan, and W. Tan, *Anal. Chem.* **78**, 2918 (2006).
- ¹⁹ K. Maehashi, T. Katsura, K. Kerman, Y. Takamura, K. Matsumoto, and E. Tamiya, *Anal. Chem.* **79**, 782 (2007).
- ²⁰ M. Pacios, I. Martin-Fernandez, X. Borrísé, M. del Valle, J. Bartroli, E. Lora-Tamayo, P. Godignon, F. Pérez-Murano, and M. J. Esplandiú, *Nanoscale* **4**, 5917 (2012).
- ²¹ S. Okuda, S. Okamoto, Y. Ohno, K. Maehashi, K. Inoue, and K. Matsumoto, *J. Phys. Chem. C* **116**, 19490 (2012).
- ²² B. K. Das, C. Tlili, S. Badhulika, L. N. Cella, W. Chen, and A. Mulchandani, *Chem. Commun. (Camb)*. **47**, 3793 (2011).
- ²³ O. A. Alsager, S. Kumar, G. R. Willmott, K. P. McNatty, and J. M. Hodgkiss, *Biosens. Bioelectron.* **57**, 262 (2014).
- ²⁴ O. A. Alsager, S. Kumar, B. Zhu, J. Travas-Sejdic, K. P. McNatty, and J. M. Hodgkiss, *Anal. Chem.* **87**, 4201 (2015).
- ²⁵ H.Y. Zheng, O. A. Alsager, C. S. Wood, J. M. Hodgkiss, and N. O. V. Plank, *J. Vac. Sci. Technol. B* **33**, 06F904 (2015).
- ²⁶ F. He, Y. Tang, S. Wang, Y. Li, and D. Zhu, *J. Am. Chem. Soc.* **127**, 12343 (2005).
- ²⁷ A.-E. Radi and C. K. O'Sullivan, *Chem. Commun. (Camb)*. 3432 (2006).
- ²⁸ B. Zhu, M. A. Booth, H. Young Woo, J. M. Hodgkiss, and J. Travas-Sejdic, *Chem. - An Asian J.* **10**, 2169 (2015).
- ²⁹ J.H. An, S.J. Park, O.S. Kwon, J. Bae, and J. Jang, *ACS Nano* **7**, 10563 (2013).
- ³⁰ G. A. Zelada-Guillén, P. Blondeau, F.X. Rius, and J. Riu, *Methods* **63**, 233 (2013).
- ³¹ Z. Chen, J. Appenzeller, J. Knoch, Y. Lin, and P. Avouris, *Nano Lett.* **5**, 1497 (2005).
- ³² I. Heller, A. M. Janssens, J. Männik, E. D. Minot, S. G. Lemay, and C. Dekker, *Nano Lett.* **8**, 591 (2008).
- ³³ H. Sun, X. Li, Y. Li, L. Fan, and H.-B. Kraatz, *Analyst* **138**, 856 (2013).
- ³⁴ J. P. Kim, B. Y. Lee, S. Hong, and S. J. Sim, *Anal. Biochem.* **381**, 193 (2008).
- ³⁵ B. Kim, I.H. Jung, M. Kang, H.K. Shim, and H.Y. Woo, *J. Am. Chem. Soc.* **134**, 3133 (2012).
- ³⁶ M. Krüger, M.R. Buitelaar, T. Nussbaumer, C. Schönenberger, and L. Forró, *Appl. Phys. Lett.* **78**, 1291 (2001).
- ³⁷ I. Heller, J. Kong, K. A. Williams, C. Dekker, and S. G. Lemay, *J. Am. Chem. Soc.* **2**, 7353 (2006).
- ³⁸ Q. Cao and J. A. Rogers, *Adv. Mater.* **21**, 29 (2009).
- ³⁹ J.D. Watson and F.H.C. Crick, *Nature* **171**, 737 (1953).
- ⁴⁰ M. Zheng, A. Jagota, E.D. Semke, B. a Diner, R.S. McLean, S.R. Lustig, R.E. Richardson, and N.G. Tassi, *Nat. Mater.* **2**, 338 (2003).
- ⁴¹ Z. Chen, L. Chen, H. Ma, T. Zhou, and X. Li, *Biosens. Bioelectron.* **48**, 108 (2013).
- ⁴² E. Stern, R. Wagner, F. J. Sigworth, R. Breaker, T. M. Fahmy, and M. A. Reed, *Nano Lett.* **7**, 3405 (2007).
- ⁴³ C.-C. Huang and H.-T. Chang, *Chem. Commun. (Camb)*. 1461 (2008).
- ⁴⁴ C. Ma, H. Huang, and C. Zhao, *Anal. Sci.* **26**, 1261 (2010).
- ⁴⁵ H. Qin, J. Ren, J. Wang, N.W. Luedtke, and E. Wang, *Anal. Chem.* **82**, 8356 (2010).
- ⁴⁶ K. Hu, Y. Huang, S. Zhao, J. Tian, Q. Wu, G. Zhang, and J. Jiang, *Analyst* **137**, 2770 (2012).
- ⁴⁷ Z. Chen, J. Guo, S. Zhang, and L. Chen, *Sensors Actuators, B Chem.* **188**, 1155 (2013).
- ⁴⁸ Z. Chen, Y. Huang, X. Li, T. Zhou, H. Ma, H. Qiang, and Y. Liu, *Anal. Chim. Acta* **787**, 189 (2013).
- ⁴⁹ X. Ji, J. Li, and C. Yang, *J. Immunoassay Immunochem.* 37 (2014).
- ⁵⁰ J. Yu, L. Zhang, X. Xu, and S. Liu, *Anal. Chem.* **86**, 10741 (2014).
- ⁵¹ C. Ocaña, M. Pacios, and M. del Valle, *Sensors* **12**, 3037 (2012).
- ⁵² A. Bini, M. Minunni, S. Tombelli, S. Centi, and M. Mascini, *Anal. Chem.* **79**, 3016 (2007).
- ⁵³ M. Zayats, Y. Huang, R. Gill, C. Ma, and I. Willner, *J. Am. Chem. Soc.* **128**, 13666 (2006).
- ⁵⁴ Z.S. Wu, C.R. Chen, G.L. Shen, and R.Q. Yu, *Biomaterials* **29**, 2689 (2008).
- ⁵⁵ I. Heller, S. Chatoor, J. Männik, M. a G. Zevenbergen, C. Dekker, and S.G. Lemay, *J. Am. Chem. Soc.* **132**, 17149 (2010).
- ⁵⁶ K. Maehashi, K. Matsumoto, Y. Takamura, and E. Tamiya, *Electroanalysis* **21**, 1285 (2009).
- ⁵⁷ J. Lee, M. Jo, T. H. Kim, J.-Y. Ahn, D. Lee, S. Kim, and S. Hong, *Lab Chip* **11**, 52 (2011).

